

# The nature of $z \sim 2.3$ Lyman- $\alpha$ emitters <sup>\*</sup>

K.K. Nilsson<sup>1,2</sup>, G. Östlin<sup>3</sup>, P. Møller<sup>4</sup>, O. Möller-Nilsson<sup>2</sup>, C. Tapken<sup>5</sup>, W. Freudling<sup>4</sup>, and J.P.U. Fynbo<sup>6</sup>

<sup>1</sup> ST-ECF, Karl-Schwarzschild-Straße 2, 85748, Garching bei München, Germany

<sup>2</sup> Max-Planck-Institut für Astronomie, Königstuhl 17, 69117 Heidelberg, Germany

<sup>3</sup> The Oskar Klein Centre for Cosmoparticle Physics, Department of Astronomy, Stockholm University, S-106 91 Stockholm, Sweden

<sup>4</sup> European Southern Observatory, Karl-Schwarzschild-Straße 2, 85748 Garching bei München, Germany

<sup>5</sup> Astrophysikalisches Institut Potsdam, An der Sternwarte 16, 14482 Potsdam, Germany

<sup>6</sup> Dark Cosmology Centre, Niels Bohr Institute, University of Copenhagen, Juliane Maries Vej 30, 2100 Copenhagen Ø, Denmark

Received date / Accepted date

**Abstract.** We study the multi-wavelength properties of a set of 171 Ly $\alpha$  emitting candidates at redshift  $z = 2.25$  found in the COSMOS field. The candidates are shown to have different properties from those of Ly $\alpha$  emitters found at higher redshift, by fitting the spectral energy distributions (SEDs) using a Monte-Carlo Markov-Chain technique and including nebular emission in the spectra. The dust contents and stellar masses are both higher, with  $A_V = 0.0 - 2.0$  mag and stellar masses in the range  $\log M_* = 9.0 - 11.0 M_\odot$ . Young population ages are well constrained, but older population ages are typically unconstrained. In 40% of the galaxies only a single, young population of stars is observed. We show that the ages and Ly $\alpha$  fluxes of the best fit galaxies are correlated with their dust properties, with higher dust extinction in younger galaxies. We conclude that the stellar properties of Ly $\alpha$  emitters at  $z = 2.25$  are different from those at higher redshift and that they are very diverse. Ly $\alpha$  selection appears to be an excellent tracer of the general galaxy evolution throughout the Universe.

**Key words.** cosmology: observations – galaxies: high redshift

## 1. Introduction

The high redshift Universe hosts a zoo of various types of galaxies, selected with many different methods. Based on numbers of detections, the by far most abundant group of star-forming galaxies with redshifts  $z > 3$  are the Lyman-Break Galaxies (LBGs; Steidel et al. 1996, 1999, Madau et al. 1996, Papovich et al. 2001, Giavalisco 2002, Ouchi et al. 2004), found by searching for the Lyman-break in the spectra of galaxies using broad-band imaging. These galaxies often turn out to be moderately star-forming, medium mass galaxies (Shapley et al. 2005; Reddy et al. 2006; Verma et al. 2007). Another large group of high redshift galaxies are found based on their red colours (DRGs, EROs; Franx et al. 2003; Daddi et al. 2004). Unlike the LBGs, and as expected from their colours, these galaxies are often massive and dusty (Förster-Schreiber et

al. 2004; Papovich et al. 2006). Other types of high redshift galaxies include star-bursting galaxies such as those detected with sub-mm arrays (SMGs; Ivison et al. 1998, 2000, Blain et al. 1999, Chapman et al. 2005) and smaller galaxies detected when gamma-ray bursts occur in them (Bloom et al. 1998, Fynbo et al. 2002, Christensen et al. 2004). One selection method that has become increasingly popular is that of narrow-band imaging for the highly redshifted Ly $\alpha$  line in star-forming galaxies (e.g. Møller & Warren 1998, Cowie & Hu 1998). The largest samples to date include several hundred Ly $\alpha$  emitters between redshifts  $z = 2 - 5$  (Gronwall et al. 2007, Venemans et al. 2007, Nilsson et al. 2007, Finkelstein et al. 2007, Ouchi et al. 2008, Grove et al. 2009, Guaita et al. 2010). Slowly, studies into the actual properties of the type of galaxies selected with this method, most notably through SED fitting, are getting under way.

There is a large spread in the results of previously published work on the topic of Ly $\alpha$  emitter properties and much work is still needed to determine what type of galaxies are

Send offprint requests to: knilsson@eso.org

<sup>\*</sup> Based on observations carried out at the European Southern Observatory (ESO) under prog. ID No. 084.A-0318(B).

selected with the Ly $\alpha$  technique, and where they belong in the high redshift galaxy zoo. To date, nine publications have presented the SED fitted properties of high redshift Ly $\alpha$  emitters (Gawiser et al. 2006, 2007; Finkelstein et al. 2007, 2009a; Lai et al. 2007, 2008; Nilsson et al. 2007; Pirzkal et al. 2007; Yuma et al. 2010), and two in the local Universe (e.g. Hayes et al. 2007; Finkelstein et al. 2009b). Ly $\alpha$  emitters are selected based on their properties in the UV and have often been found to be extremely faint at longer wavelengths. Since the UV light is dominated by young stars, also contributing to the Ly $\alpha$  emission, little is thus known about the properties of any underlying populations of stars. For galaxies above redshift two, it is thus crucial to have detections of the galaxies in the near- and mid-IR, corresponding to restframe optical and near-IR wavelengths. Few Ly $\alpha$  emitters have been detected in these wavelength regimes, with only a handful to date at  $z \sim 3$  (Lai et al. 2008), and at  $z = 4 - 6$  (Lai et al. 2007, Pirzkal et al. 2007, Finkelstein et al. 2008, 2009a, Yuma et al. 2010). These studies have shown IR-detected Ly $\alpha$  emitters to be in general more massive, and in some cases more dusty than their non-IR-detected counter-parts. It is not yet clear whether there are indeed two (or multiple) populations of Ly $\alpha$  emitters (e.g. faint-small-dust-free vs. bright-massive-dusty) or if there is a smooth transition of objects with various masses and properties.

The surveys to date have concentrated on redshifts  $z > 3$ . In an effort to get a better handle on the SED of the selected galaxies, we here present the SED study of a sample of Ly $\alpha$  emitters at lower redshift,  $z = 2.25$ , first presented in Nilsson et al. (2009a). The advantages of the lower redshift include the possibility of observing a larger range of the restframe spectra with the same instruments and increased signal-to-noise in the detections due to the smaller luminosity distance. Several signs of evolution in the properties of this type of galaxy from redshift  $z \sim 3$  to  $z \sim 2$  were reported in Nilsson et al. (2009a); including typically redder colours, smaller equivalent widths and a larger AGN content in the sample. In this paper we investigate the stellar properties of the LAEs further by fitting their SEDs with theoretical models. The questions we seek to answer are how these properties have evolved from higher to lower redshift.

This paper is organised as follows: section 2 describes the sample of Ly $\alpha$  emitters that are being studied, and includes an analysis of the Spitzer detections of the galaxies. In section 3 we outline the method used for the SED fitting, and the results of the fitting are reported in section 4. A discussion of the redshift evolution of LAE stellar properties is found in section 5. We end with a general discussion in section 6 and a conclusion in section 7.

Throughout this paper, we assume a cosmology with  $H_0 = 72 \text{ km s}^{-1} \text{ Mpc}^{-1}$ ,  $\Omega_m = 0.3$  and  $\Omega_\Lambda = 0.7$ . Magnitudes are given in the AB system.

## 2. Data

### 2.1. Sample

The sample studied in this paper is nearly identical to the sample in Nilsson et al. (2009a). In brief, this sample was found through narrow-band imaging with the ESO2.2m/MPG telescope on La Silla, Chile, using the Wide-Field Imager (WFI; Baade et al. 1999). A central section of the COSMOS field (R.A.  $10^h00^m27^s$ , Dec  $02^\circ12'22''.7$ , J2000) was observed with the filter N396/12, observing Ly $\alpha$  with  $z = 2.206 - 2.312$ . The data reduction and method for selecting emission line objects is explained in detail in Nilsson et al. (2009a). In the survey, 187 emission-line objects were found. Of these, 17 were detected in the public GALEX data available and were flagged as potential [OII] emitters, although this sub-sample will also contain Ly $\alpha$  emitters with high escape fraction in the restframe UV. After removing the GALEX detected objects, a list of 170 robust LAE candidates remained. The photometry of these candidates in the optical and near-infrared data available in COSMOS is presented in Nilsson et al. (2009a).

In January/February 2010, multi-object spectroscopy with the VIMOS instrument on VLT UT3 (programme ID 084.A-0318(B)) was carried out on 152 of the candidates. The results of this spectroscopic campaign will be presented in a forthcoming publication, but we will in the analysis here exclude those candidates which are clearly confirmed to not be Ly $\alpha$  emitters in the spectroscopy (a total of 22, of which 4 were AGN, 2 were GALEX-detected, and 3 were both). Conversely, a number of less likely (named “unlikely” in Nilsson et al. 2009a) candidates were put on slits. Those that showed a Ly $\alpha$  detection in the spectroscopy will be added to the analysis here (a total of six). The results of the Nilsson et al. (2009a) paper do not change significantly from the exclusion/inclusion of the spectroscopic rejections/confirmations.

### 2.2. Updated photometry

Since the publication of the sample, several new images have become available from the COSMOS consortium, including J images from UKIRT,  $K_s$  images from CFHT and X-ray data from the *Chandra* observatory (see sec. 2.3). The depth of the infrared images are 23.7 magnitudes ( $5\sigma$ ) in both bands (Ilbert et al. 2009). We prepared and extracted fluxes of all the objects in the catalogue in a similar way as described in Nilsson et al. (2009a). The number of detections was 43 and 86 of the 171 candidates respectively in the J and  $K_s$  bands. One of the spectroscopically confirmed less likely candidates was detected in the  $K_s$  band. These results were incorporated into our main photometric catalogue. In the case that an object was already detected in the previously available, but shallower, KPNO  $K_s$  band, this magnitude was replaced with the CFHT result for consistency.

### 2.3. *Chandra* detections

Elvis et al. (2009) presented the available *Chandra* X-ray images, with a flux limit of 1.9, 7.3 and  $5.7 \times 10^{-16} \text{ erg s}^{-1} \text{ cm}^{-2}$

**Table 1.** S-COSMOS sensitivities from Sanders et al. (2007).

Band	CWL	FWHM	Sensitivity
Ch1	3.58	0.75	0.0009
Ch2	4.50	1.02	0.0017
Ch3	5.80	1.43	0.0113
Ch4	8.00	2.91	0.0146
MIPS (deep)	24.0	4.7	0.071
MIPS (shallow)	24.0	4.7	0.15

Central wavelengths and full width half maximums are given in  $\mu\text{m}$ . Sensitivities are  $5\sigma$ , and given in mJy. Only MIPS 24  $\mu\text{m}$  values are given as our candidates have no detections in the longer wavelength bands.

in the soft (0.5 – 2 keV), hard (2 – 10 keV) and total (0.5 – 10 keV) bands respectively. To search for detections, aperture photometry on the positions of the candidates was made in the 0.5 – 10 keV band. For detections at the  $3\sigma$  level, the photometry was repeated in the soft and hard bands. This revealed 26 detections, of which six are only detected in the total band, seven/one are detected in the total and soft/hard bands. Twelve candidates are detected in all bands. Now we have a total of 24 LAE AGN, 11 of which are only detected with *Chandra*, three are only detected in radio emission with VLA, one is only detected with XMM, and 9 that are detected by both *Chandra* and VLA/XMM. The new AGN detections are LAE\_COSMOS# 14, 20, 29, 52, 67, 76, 120, 130, 134, 151 and 175. Thus the confirmed AGN contamination in the non-GALEX-detected sample (taking into account the results of the spectroscopy) is increased from 5% to at least 13%, a much larger percentage than in high redshift samples (Wang et al. 2004, Gawiser et al. 2007) although samples of Ly $\alpha$  emitters at  $z = 0.3$  and  $z = 2.2$  has been shown to contain a large AGN fraction ( $\sim 43\%$  at  $z = 0.3$ , Finkelstein et al. 2009c, and  $\sim 75\%$  at  $z = 2.2$ , Bongiovanni et al. 2010) indicating a clear redshift evolution. The LAE AGN have total X-ray fluxes between  $\log L_{0.5-10\text{keV}} = 43.3 - 45.5 \text{ erg s}^{-1}$ , if at  $z = 2.25$ . Their R band-to-X-ray fluxes are in the range of what is commonly found for AGN, hence the X-ray detected LAEs are AGN and not starburst galaxies (Schmidt et al. 1998, Hornschemeier et al. 2001).

#### 2.4. Spitzer detections

The COSMOS field is covered by *Spitzer* in the S-COSMOS survey (Sanders et al. 2007). The public data includes the four IRAC channels (3.6, 4.5, 5.8 and 8.0  $\mu\text{m}$ ), and the three MIPS bands (24, 70 and 160  $\mu\text{m}$ ). We will not discuss the 70 and 160  $\mu\text{m}$  bands further as no detections were made in those bands. In the MIPS 24  $\mu\text{m}$  band, both a full and a deep survey have been published, with the deep survey covering roughly 33% of the original narrow-band image used for selection of candidates. The sensitivities of the *Spitzer* data can be found in Table 1. We searched the public catalog for sources associated with our candidates. In the IRAC bands, counterparts

were searched for within a circle with 5 IRAC pixels ( $3''$ ) radius around each candidate, and in the MIPS bands within a circle with 4 MIPS pixels ( $8.8''$ ) radius. In total [58, 49, 24, 18, 8] candidate counterparts were found in the [Ch1, Ch2, Ch3, Ch4, MIPS-24] bands, see also Table 2 that includes all subsets of the candidates. The random probability of finding an object within our search radii are 0.0096 in Ch1, resulting in 1.8 random false detections in the whole sample. After visually inspecting the associations, two were excluded as random false detections and the list of Spitzer detected sources should, after removal of these two sources (detected in Ch1 and Ch2), be robust. The detection rate of our candidates is 34% in Ch1 and 5% in MIPS-24, which is a higher rate than found in surveys for LAEs at redshifts three and beyond (Lai et al. 2007, 2008) but in agreement with surveys at  $z \sim 2.3$  (Colbert et al. 2006). The MIPS-24 detected candidates are by definition also ultra-luminous infrared galaxies (ULIRGs) due to their bright infrared fluxes. For a further discussion on these LAE ULIRGs, see Nilsson & Møller (2009).

To test the public catalogues we performed aperture photometry on a number of objects in the catalogue. The catalogue fluxes were extracted in  $1''.4$  radius apertures (to be compared to  $1''.5$  radius apertures for the optical broad-band images). The fluxes measured in the image were in reasonable agreement with the catalogue values, however, the errors measured were in the cases of Ch1 - Ch3 roughly two times those quoted in the catalogue. For Ch4 and MIPS the errors were also in agreement. Thus we multiply the published errors on our candidates in the Ch1 - Ch3 bands by two for the following analysis. There was a slight tendency of over-estimation of the fluxes in Ch1, however, it was not significant enough to warrant a correction of the catalogue fluxes. It should be noted though, that the Ch1 fluxes may be over-estimated by up to 5%. In the subsequent SED fitting, an extra error of 10% of the flux of each object was included, in order to account for systematic errors in the data reduction (see also Muzzin et al. 2009).

### 3. SED fitting method

The method used to fit the SEDs of the LAEs is an updated version of the code used in Nilsson et al. (2007). It is based on the stellar populations catalogue GALAXEV (Bruzual & Charlot 2003) and the fitting is done using a Monte-Carlo Markov-Chain (MCMC) algorithm. The algorithm explores a multi-dimensional parameter space by stepping in a random fashion from one point  $P_i$  in this space to another  $P_{i+1}$ . The step is random in the sense that the projected distance from point  $P_i$  to  $P_{i+1}$  along one of the parameter axis in the parameter space is a randomly chosen value ranging from 0 to the maximum step size,  $\Delta P_{max}$ . The direction of the step along an axis is also random, with a probability of 50% that the direction is along the positive or negative direction respectively. We impose boundary conditions for all parameters and ensure that no step leads to a value outside these boundaries. The parameters and the boundary values we impose on them are listed in Table 3. Once a new point  $P_{i+1}$  is determined, the current model is advanced to the new point with a probability  $p_{i \rightarrow i+1}$  which is given by

**Table 2.** Spitzer detections for all sub-sets of LAE candidates.

Band	Total sample	LAE best	GALEX only	AGN only	GALEX + AGN
Ch1	58 (34%)	38 (27%)	3 (38%)	13 (65%)	4 (100%)
Ch2	49 (29%)	31 (22%)	2 (25%)	12 (60%)	4 (100%)
Ch3	24 (14%)	9 (6%)	0 (10%)	11 (55%)	4 (100%)
Ch4	18 (11%)	6 (4%)	0 (10%)	9 (45%)	3 (75%)
MIPS	8 (5%)	4 (3%)	0 (0%)	2 (10%)	2 (50%)

The sub-set of the LAE candidates are: the total sample, the sample of candidates without GALEX or AGN signatures, the GALEX and AGN only detections. The total sample consists of 171 candidates of which 139 are LAE best candidates, 8 only GALEX detected, 20 only have AGN signatures, 4 have both GALEX detections and AGN signatures. Percentages of each sample are given in parentheses.

the ratio of the two model probabilities given the data  $D$ ,

$$p_{i \rightarrow i+1} = \frac{p(P_{i+1}|D)}{p(P_i|D)} = \text{Max}(\exp[(\chi_{i+1}^2 - \chi_i^2)/T], 1), \quad (1)$$

where  $\chi_{i+1}^2$  and  $\chi_i^2$  are the reduced  $\chi^2$  values for the two points in the parameter space and  $T$  is a “temperature” parameter which can be used to adjust the convergence. In our case  $T = 1$ . If the model is not advanced to the new point, the parameters remain  $P_i$ , so  $P_{i+1} = P_i$ . The algorithm we use has several advantages over more common maximization algorithms (such as steepest descend, amoeba, etc.) in that it allows a full exploration of the parameter space. The result of our algorithm after  $N$  iterations is a list of points  $P_i, i = 0..N$  that, if  $N$  is sufficiently large, represents a good sample from the underlying probability distribution function of the parameters.

### 3.1. Improvement on models

Recent results show that nebular emission lines can play an extremely important role in fitting SEDs (Zackrisson et al. 2008, Schaerer & de Barros 2009, Raiter et al. 2010). In order to properly take into account this potentially large effect of gas emission in young, star-bursting galaxies, an add-on to the GALAXEV code was created. The nebular gas contributes with a continuum component and an emission-line component. The continuum addition was calculated from the Starburst99 models (Leitherer et al. 1999) with a Salpeter IMF with slope  $\alpha = 2.35$  in the mass range  $1 - 100 M_\odot$  (the Salpeter IMF is also used in the GALAXEV models). The emission-line strengths were calculated using the MAPPINGS photoionisation code (Kewley et al. 2010, in prep.). Both nebular continuum and emission-line strengths were calculated on a grid of ages (for the continuum in 36 steps between 1 and 100 Myrs and for the emission lines in six steps between 1 and 20 Myrs) and metallicities (same as available in GALAXEV, see below) and for each fit, the nearest values for these parameters were used. The emission-lines were scaled with the H $\alpha$  flux and the number of ionising photons in the galaxy spectra produced by GALAXEV. For an illustration of the added nebular emission, see Fig. 1. In practice, the emission line strengths as well as the continuum contribution become negligible at ages  $\gtrsim 20$  Myrs.

In this publication, we choose to fit only two single stellar populations (SSP) models, as the nebular emission add-

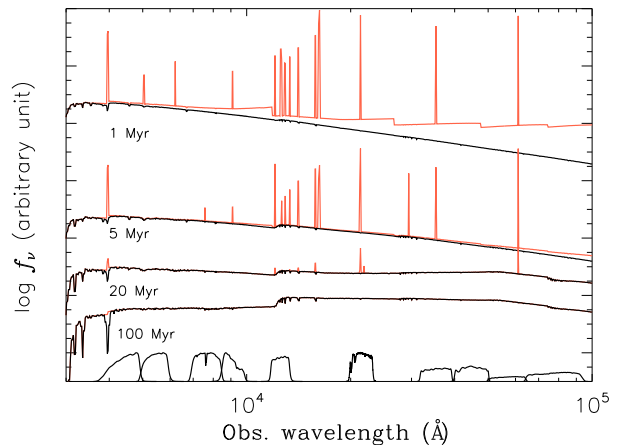


**Fig. 1.** Illustration of the added nebular emission. GALAXEV spectra at  $z = 2.25$  with ages 1, 5, 20, and 100 Myrs are shown with nebular emission lines (red) and without (black). The spectra are scaled to arbitrary units to illustrate the effect of age on the nebular emission. The filtercurves of the filters used in the fitting (Bj, Vj,  $i^+$ ,  $z^+$ , J,  $K_s$  and Spitzer Ch1-4) are shown at the bottom of the figure. The nebular emission lines are added as delta functions at the respective wavelength of the emission lines, and the step-like appearance of the 1 Myr spectrum is due to the nebular continuum emission. At ages larger than 20 Myrs, the effect of the nebular add-on becomes negligible.

on becomes too complicated with any other star formation history. For all models, dust is added according to Calzetti et al. (2000). The parameter space allowed is detailed in Table 3. For the metallicity, the steps allowed are  $Z/Z_\odot = 0.005, 0.02, 0.2, 0.4, 1.0$ . Only fluxes in the bands from Bj to the  $8.0\mu\text{m}$  bands are used, as there are large uncertainties in the models at wavelengths below the Ly $\alpha$  line, and at restframe mid-IR wavelengths.

When the spectrum of a very young SSP is added with an older SSP spectrum, the older spectrum will need to comprise a very large mass fraction in order to be seen, as the young SSP will dominate the total spectrum. To test at what mass fractions the old population is actually seen, several young and old SSPs



**Table 3.** Parameter space allowed by SED fitting code.

	Min	Max	Remark
Old pop. age	0 Gyr	2.7 Gyr	
Young pop. age	0 Gyr	0.1 Gyr	< Old age
Mass frac. in young pop.	0	1	
Dust $A_V$	0 mag	5 mag	
Metallicity $Z/Z_\odot$	0	1.0	In steps, see text
Stellar Mass	—	—	Free parameter

were generated and co-added with different mass fractions. To find a criterium for whether the older population is observable, the colour in V $_j$ –IRAC Ch1 was calculated. This was compared to the typical  $1\sigma$  error bar in the photometry in these two bands. We calculated the colour significance according to:

$$col.signif.(mf) = \frac{(V_j - Ch1)_{mf} - (V_j - Ch1)_{mf=1.0}}{0.11} \quad (2)$$

where  $mf$  is the mass fraction. The number in the denominator is the typical error on the colour based on the data at hand. If this colour significance is more than  $1\sigma$ , the old population is considered to be observed. A plot of these limits can be found in Fig. 2. Based on this figure, all objects with more than 90% of its data-points above the fitted lines are considered to be single young populations.

## 4. Results

First we stacked the candidates in three different, light-weighted stacks for the fitting; the total sample without KPNO  $K_s$  detections, as well as the total sample without KPNO  $K_s$  detections divided into a “red” and a “blue” sample (with V $_j$ – $i^+$  colours greater or less than zero respectively). These stacks are identical to those in Nilsson et al. (2009a), but updated with new photometry from the UKIRT J and CFHT  $K_s$  images. The stack of KPNO  $K_s$  detected sources is excluded here as only three objects remained in stack after removing new AGN detections and spectroscopic rejections. The magnitudes for the three samples can be found in Table 4. Secondly, we also fit all individual objects with at least one detection in the Spitzer bands and/or in the  $K_s$  band. This sample consists of a total of 76 objects (58 with Spitzer detections and 18 with only a  $K_s$  detection).

For the main results presented here, the Monte Carlo Markov Chain SED fitting code was run with 10 000 iterations, and fitted the data with two populations of single stellar populations. To find the probabilities in the parameter space, the first 2000 runs were omitted to allow the  $\chi^2$  to level out. The best fit parameter is determined to be the median of the remaining 8000 fits, and the error bars are calculated by integrating to 68% of each wing of the distribution (see also Nilsson et al. 2009b). The full set of results of this run are found in Table 5. When interpreting the dust parameter,  $A_V$ , it is important to keep in mind that this is a galaxy averaged dust absorption. Different parts of the galaxy will be observable at different wavelengths. The results found here for the dust parameter will

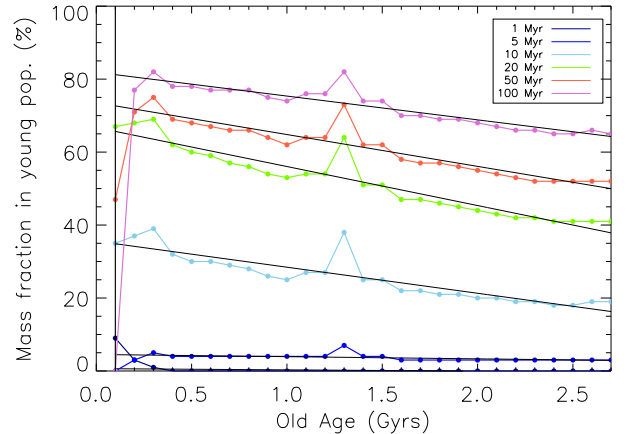


**Fig. 2.** Mass fractions of the young populations at which an old population is discernible from a young population. Galaxies with mass fractions fit *below* these lines have two observable populations, for those with mass fractions fit *above* the lines it is impossible to discern any older population. The limiting mass fraction where the older population becomes visible are shown with different colours, depending on the ages of the young population. At very young ages of the young population, all older populations are invisible. The solid vertical line marks the age limit of the young population in our fits. The solid horizontal lines are linear fits to the limiting mass fraction dependencies on the older population age. The peak at age  $\sim 1.3$  Gyrs is a numerical artifact due to the limited age grid in the GALAXEV models. This does not affect our results as we use the solid, fitted lines for the measurements.

be dominated by the absorption of the restframe UV part of the spectrum, see also section 4.2.1.

When doing SED fitting, many of the parameters that are fit for can be degenerate with other parameters. In Fig. 3 we show, as an example, the contours of probability for the parameters of old population age, mass fraction in the young population, dust  $A_V$ , stellar mass, and young population age for two example objects (LAE\_COSMOS\_52 and 131), one that has a single young population and one that has a detectable older population (see also section 4.2). Of the parameters fitted for, the stellar mass is the best constrained. Secondly, the dust  $A_V$  is also well fit. Age of the old population, mass fractions and metallicities are the least constrained parameters. As can be seen in Fig. 3, our calculation of the best fit value and its error bars is a good estimate of the distribution of parameters. No clear dependencies are seen. We will hereafter not discuss metallicities further, as they are in almost all cases completely unconstrained.

### 4.1. Stack results

The results for the stacked samples are shown in Table 5 (top). A general comment for all results, both stacked and individual, is that the old population age is very hard to constrain and the

**Table 5.** Full results of SED fitting run. **This table will be in electronic format only. It can be requested from the authors.**

Stacked samples									
Stack	Old Age Gyrs	Young Age Gyrs	Mass frac. (in young)	Dust $A_V$	Metallicity $Z/Z_\odot$	$\log M_*$ $M_\odot$	$\chi_r^2$	SFR $_{corr}$ $M_\odot \text{ yr}^{-1}$	AGN/GAL
Total non- $K_s$	$1.24^{+1.02}_{-0.83}$	$0.07^{+0.02}_{-0.05}$	$0.56^{+0.32}_{-0.22}$	$0.28^{+0.46}_{-0.16}$	$0.4^{+0.6}_{-0.2}$	$9.83^{+0.15}_{-0.17}$	$2.48^{+1.05}_{-0.63}$	—	
Red	$1.31^{+0.91}_{-0.67}$	$0.07^{+0.02}_{-0.05}$	$0.46^{+0.30}_{-0.18}$	$0.43^{+0.57}_{-0.21}$	$0.4^{+0.6}_{-0.2}$	$10.12^{+0.13}_{-0.27}$	$4.02^{+0.99}_{-0.74}$	—	
Blue	$1.47^{+0.75}_{-1.02}$	$0.05^{+0.02}_{-0.03}$	$0.76^{+0.19}_{-0.32}$	$0.12^{+0.25}_{-0.09}$	$0.4^{+0.6}_{-0.38}$	$9.34^{+0.18}_{-0.18}$	$4.05^{+1.65}_{-1.55}$	—	
Individual results									
1	—	$0.02^{+0.00}_{-0.00}$	$> 0.52$	$1.18^{+0.08}_{-0.20}$	$1.00^{+0.00}_{-0.60}$	$9.86^{+0.06}_{-0.15}$	$5.80^{+0.86}_{-0.60}$	$36.50 \pm 2.30$	
8	$0.07^{+0.75}_{-0.02}$	$0.05^{+0.03}_{-0.02}$	$0.02^{+0.11}_{-0.01}$	$0.58^{+0.17}_{-0.57}$	$0.40^{+0.60}_{-0.20}$	$10.04^{+0.15}_{-0.18}$	$146.81^{+17.71}_{-22.13}$	—	
11	$0.73^{+1.39}_{-0.03}$	$0.08^{+0.01}_{-0.00}$	$0.85^{+0.14}_{-0.02}$	$1.34^{+0.30}_{-0.05}$	$0.40^{+0.60}_{-0.00}$	$10.72^{+0.01}_{-0.00}$	$19.33^{+4.71}_{-0.00}$	—	
14	$0.53^{+0.22}_{-0.02}$	$0.07^{+0.00}_{-0.00}$	$0.90^{+0.07}_{-0.00}$	$1.70^{+0.07}_{-0.00}$	$0.02^{+0.18}_{-0.00}$	$11.23^{+0.08}_{-0.00}$	$67.20^{+2.19}_{-0.20}$	—	A
15	$0.41^{+1.46}_{-0.34}$	$0.07^{+0.03}_{-0.03}$	$0.84^{+0.06}_{-0.31}$	$0.64^{+0.65}_{-0.15}$	$0.40^{+0.60}_{-0.20}$	$10.36^{+0.28}_{-0.14}$	$8.91^{+2.94}_{-1.23}$	$23.04 \pm 1.17$	

Columns show medians and 68% confidence levels on each parameter fit in the SED runs. Ages are in Gyrs and the mass fraction is the fraction of the total mass in the young population. Metallicity is fitted in steps, see the text for a description. The  $\chi_r^2$  is the reduced chi-square. The eighth column gives the dust corrected UV star formation rates for the candidates with  $\chi_r^2 < 10$ , see also sec. 4.3. The final columns marks the entry with a G if the object is detected in the GALEX images, and an A if it is detected in the public X-ray and/or radio data.

**Table 4.** Magnitudes for fitting of the stacked SEDs.

	Total non- $K_s$	“Red”	“Blue”
#	144	96	48
B <sub>j</sub>	$25.14 \pm 0.03$	$25.11 \pm 0.04$	$25.34 \pm 0.05$
V <sub>j</sub>	$24.99 \pm 0.08$	$24.89 \pm 0.11$	$25.18 \pm 0.05$
$i^+$	$24.95 \pm 0.14$	$24.72 \pm 0.13$	$25.37 \pm 0.15$
$z^+$	$24.86 \pm 0.22$	$24.57 \pm 0.15$	$25.40 \pm 0.16$
J	$23.95 \pm 0.24$	$23.63 \pm 0.22$	$24.54 \pm 0.45$
$K_s$	$23.61 \pm 0.10$	$23.27 \pm 0.08$	$24.50 \pm 0.18$
Ch1	$23.75 \pm 0.14$	$23.23 \pm 0.12$	$24.67 \pm 1.89^*$
Ch2	$23.59 \pm 0.10$	$23.11 \pm 0.09$	$24.83 \pm 2.13^*$
Ch3	$23.38 \pm 0.42$	$22.80 \pm 0.12$	$23.41 \pm 2.40^*$
Ch4	$23.58 \pm 0.41$	$22.95 \pm 0.19$	$26.54 \pm 2.94^*$

First row gives number of galaxies in stack. Errors are the largest of either the background variance noise or the result of bootstrapping error calculation. \*Magnitudes marked with a star for the blue sample have been calculated from the combined measurements of the total and red stacks.

error bars are typically several hundred Myrs. There is a large consistency between the stack results. The old/young ages are similar between the stacks. As expected, the red versus blue stacks display diverging properties in dust and mass, with the red stack being dustier and more massive ( $A_V = 0.43$ ,  $M_* = 1.3 \times 10^{10} M_\odot$ ) than the blue stack ( $A_V = 0.12$ ,  $M_* = 2.2 \times 10^9 M_\odot$ ). The total stack has values in between those of the red and blue stack results. The results of these three stacks are also well fitted, with  $\chi_r^2 < 5$ .

## 4.2. Individual results

The values of the best fit parameters for all individually fitted objects are found in Table 5 (bottom). We will in this section remark on the general properties of all these objects, and on one special case. Of the, in total 76, objects fitted, four are detected in the GALEX data (and thus flagged as potential interlopers), eleven are detected as AGN in the X-ray or radio data and four are both AGN- and GALEX-detected. For the objects detected as AGN, marked with an A in Table 5, the fit is merely done for reference, as the SED is affected by an unknown amount of light from the central AGN. It is not surprising that several of them have relatively high  $\chi_r^2$ . In Fig. 4 the histogram of the best fit  $\chi_r^2$  are shown. An obvious break is seen at  $\chi_r^2 \approx 10$  in the distribution. In Fig. 5, three examples of SEDs and best fit spectra with very different  $\chi_r^2$  are shown. With so many data-points to fit, taken from such disparate sources, the fit becomes challenging. It is clear though that fits with  $\chi_r^2 \approx 10$  still appear to be very good fits, as seen in the example of LAE\_COSMOS\_183, Fig. 5. If we remove the candidates that are AGN selected, 36 of the remaining 61 candidates have  $\chi_r^2 < 10$ . None of these candidates are GALEX-detected. For the remaining candidates with very bad  $\chi_r^2$ , about half have Spitzer data points lying significantly off from the other SED points (see e.g. LAE\_COSMOS\_81, Fig. 5), and the other half have unusual SEDs, possibly consistent with lower redshift. Because of the reasons mentioned above, the results for the galaxies with bad  $\chi_r^2$  are not reliable and we will concentrate on the 36 candidates with  $\chi_r^2 < 10$  and which are neither AGN- nor GALEX-detected in the further analysis.

For all galaxies, the test shown in Fig. 2 was performed in order to determine if a galaxy was best described by two stellar populations, or could be best fitted with a single young population of stars. Hereafter, the “Age” of a galaxy is considered to be the age of the young population, if no older population can be seen, and the age of the older population, if this is con-

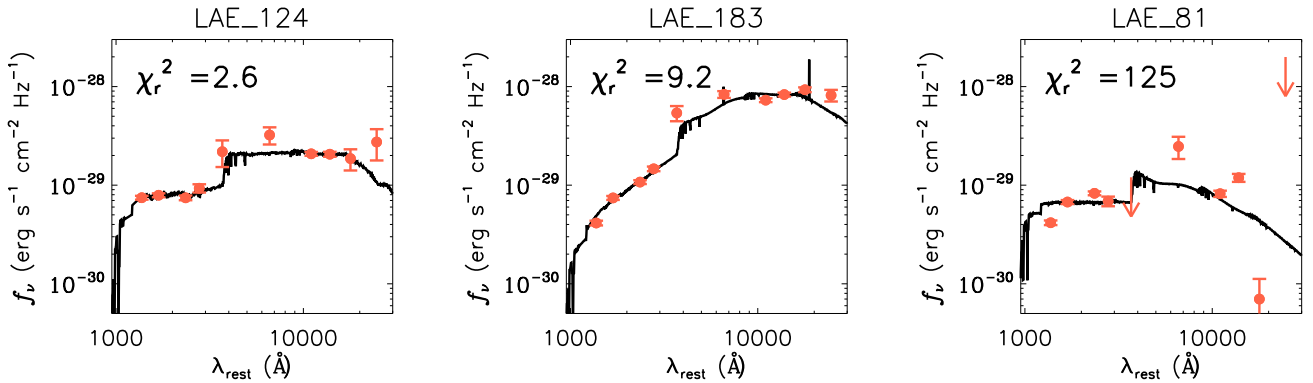


**Fig. 5.** Illustration of the goodness of fit with various  $\chi_r^2$  from three candidates. The  $\chi_r^2$  are 3, 9 and 125 respectively from left to right in the figure. As can be seen, also fits with  $\chi_r^2 \sim 10$  are reasonably good fits.

sidered observed (cf. Fig. 3). The results from the SED fits can be found in Fig. 6. As can be seen in this figure,  $\sim 40\%$  of the galaxies exhibit single young populations. Conversely,  $\sim 60\%$  can be seen to hold at least one population of older stars. This is similar to the results of Guaita et al. (2010). If the stellar mass in the two sub-samples is summed up, 17% of the total stellar mass is in the young galaxies, and 83% is in the old. Hence, the stellar mass per galaxy is on average higher in those galaxies with an older population. The older ages of these multiple population galaxies range between 0.5 – 2 Gyr with a mean of  $1.2 \pm 0.16$  Gyrs, but are relatively unconstrained. The ages of the single, young population galaxies are  $25 \pm 4$  Myrs. The dust  $A_V$  values for the whole sample range between 0.0 – 1.5 mag, with mean  $A_V = 0.48 \pm 0.05$  mag and  $0.96 \pm 0.07$  mag for the old and young populations. The stellar masses are in the range  $8.5 < \log M_* < 11 M_\odot$ , with, for the old/young populations,  $\log M_* = 10.4 \pm 0.03 / 10.1 \pm 0.1 M_\odot$ . In Table 5, the lower limits are given on the mass fractions in the young population in those galaxies with a single young population observed.

When fitting SEDs at higher redshift, typically many objects are stacked in order to increase the signal-to-noise of the photometric measurements. But the question remains if the properties found fitting such a stack will be the average properties of the individual objects. To test this with our data, the 36 best fit objects were stacked, and the stack fitted in an identical way as for the individual objects. The results gave the parameters (old population) age  $1.05_{-0.52}^{+0.88}$  Gyrs,  $A_V = 0.34_{-0.23}^{+0.22}$  mag, and stellar mass  $\log M_* = 10.37_{-0.12}^{+0.13} M_\odot$ . These values are very similar to the mean values among those detected to have an older population individually; the stellar masses and ages are almost in perfect agreement, and the  $A_V$  is slightly lower for the stack than for the mean of the older population objects. Conversely, the younger ages, and the higher  $A_V$ , of the single young population objects appear to be invisible in the stack. The result can be understood from the fact that the stack is a light-weighted mean of all SEDs. The older, more massive, objects will dominate this stack, and it becomes impossible to know whether some objects in the stack are indeed dominated by one young population of stars.

#### 4.2.1. LAE ULIRGS

It was shown in Nilsson & Møller (2009) that some of these candidates had infrared fluxes consistent with being ultra luminous infrared galaxies (ULIRGs). We now ask the question if these galaxies are located in a certain part of the parameter space fitted, or if they are evenly distributed. Of the non-AGN ULIRGs in the sample, four were fitted with good  $\chi_r^2$  and these are marked with a red ring in Fig. 6. They appear evenly distributed throughout the diagrams. Further, they are generally above the average in stellar mass and all contain a significant older stellar population, but are very evenly distributed in the extinction parameter. The extinction in the UV/optical ( $A_V$ ) was derived from the ratio of UV to infrared fluxes in Nilsson & Møller (2009), and ranged between 4.8 – 7.2 magnitudes for the four that have been fitted here. Clearly, the two methods, of determining the dust extinction primarily based on the UV slope compared to including infrared data points, reveal vastly different extinction values.

#### 4.2.2. LAE\_COSMOS\_94

One very interesting example of the LAE ULIRGs is LAE\_COSMOS\_94, fitted with a best  $\chi_r^2 = 8.2$ . This object, which is confirmed to be a Ly $\alpha$  emitter by the spectroscopy, is the one in our survey with by far the highest equivalent width ( $EW_0 = 768 \text{ \AA}$ ). It has a Ly $\alpha$  magnitude of  $24.33 \pm 0.10$  but is very faint in the optical broad-bands with magnitudes  $\sim 26$  and is even undetected in the  $z^+$  and J bands, but then shows a very red SED in the  $K_s$  and *Spitzer* bands, see Fig. 7. The best fit properties of this galaxy are age =  $1.22_{-0.79}^{+0.81}$  Gyr,  $A_V = 1.48_{-0.18}^{+0.10}$ , and  $\log M_* = 10.61_{-0.09}^{+0.17} M_\odot$ . These properties are very similar to the average properties of all the candidates, except it has one of the largest  $A_V$  of all.

Very high Ly $\alpha$  EWs have been proposed to be signs of Population III stars (Schaerer 2003, Tumlinson et al. 2003), whereas LAE\_COSMOS\_94 is obviously not a Population III object. Very high EWs could also appear in dusty objects, where the dust geometry allows Ly $\alpha$  photons to escape (cf. Finkelstein et al. 2008). This object also appears to be quite

**Table 6.** Results for the Spearman rank test on several parameter correlations.

Parameters	Spearman rank $\rho$	Correlation prob.
mass – $A_V$	–0.01	45%
age – $A_V$	–0.53	99.97%
mass – age	–0.003	44%
Ly $\alpha$ Flux – mass	–0.16	76%
Ly $\alpha$ Flux – $A_V$	–0.31	94.8%
Ly $\alpha$ EW – mass	–0.16	76%
Ly $\alpha$ EW – $A_V$	–0.05	56%

The Spearman rank number is a measure of the correlation in the data. Points along a perfectly monotonic function would have a Spearman rank of  $\pm 1$ . A positive rank number means a positive correlation between the parameters, and a negative number an anti-correlation between the parameters.

extended in the narrow-band image, with a PSF-subtracted FWHM of  $2''.04$ , corresponding to 16 kpc at  $z = 2.25$ . The PSF-subtracted FWHM in the Bj/ $r^+$  bands are  $1''.28/1''.04$ , or 10/8 kpc. The narrow-band, i.e. Ly $\alpha$  emission, is clearly more extended than the broad-band component, as has previously been found for other LAEs at both low redshift (Östlin et al. 2009) and at high redshift (Møller & Warren 1998, Fynbo et al. 2001, Finkelstein et al. 2010). This is further evidence that the high EW in this object is driven by resonant scattering, as the Ly $\alpha$  emission is expected to be more extended than the continuum emission in those cases (Östlin et al. 2009).

#### 4.2.3. Correlations in the data

To test if any correlations exist between the typical parameters stellar mass, dust  $A_V$  and age in the full sample, a Spearman rank test was performed. The Spearman rank test allows to test the existence of any monotonous relationships in the data. The results of the Spearman rank test can be found in Table 6. An anti-correlation of 99.97% significance was found between the dust attenuation and age (decreasing age with increasing dust amount).

With the data at hand, it is also possible to study dependencies between the Ly $\alpha$  fluxes and equivalent widths (EWs) and the parameters in the SED fit. In Fig. 8, the Ly $\alpha$  fluxes and EWs of the galaxies are shown as function of stellar masses and dust  $A_V$ . In the top panels in this figure, the Ly $\alpha$  flux is shown as a function of stellar mass and dust parameter. A lack of objects with large Ly $\alpha$  flux and large dust  $A_V$  is seen in the top right panel. In the lower panels of Fig. 8, the Ly $\alpha$  rest-frame EW is shown as a function of stellar mass and dust. The object with extremely high EW is LAE\_COSMOS\_94, an LAE ULIRG, see also sec. 4.2.2. No correlation between stellar mass and EW is seen, as proposed in Pentericci et al. (2009). The Spearman rank test was applied also to these data-sets, revealing only an anti-correlation ( $\sim 2.2\sigma$ ) between Ly $\alpha$  flux and  $A_V$ , see Table 6.

#### 4.3. Dust corrected star formation rates

When the dust absorption for each galaxy is determined, the UV spectrum can be corrected and the intrinsic UV flux retrieved. From the intrinsic fluxes, dust corrected star formation rates (SFR) can be derived according to the conversion of Kennicutt (1998). The uncorrected SFRs were presented in Nilsson et al. (2009a), where the UV-derived SFRs of all candidates were found to be in the range  $1 - 40 M_\odot \text{ yr}^{-1}$ . For the galaxies with good fits to the SED, the Vj band (used for the SFR calculation) can be corrected with the best fitted  $A_V$ . Within this sub-sample of 36 galaxies, the maximum SFR<sub>UV</sub> before correction was  $15 M_\odot \text{ yr}^{-1}$  and the median  $\sim 8 M_\odot \text{ yr}^{-1}$ . After correction, the range of SFRs in this sub-sample is  $3-80 M_\odot \text{ yr}^{-1}$ , with a median of  $15 M_\odot \text{ yr}^{-1}$ . These values are more similar to  $z \approx 2$  galaxies (such as BX/BM, BzK and DRG galaxies), although still in the lower two-thirds of the range covered by those galaxies (Reddy et al. 2005). The dust corrected star formation rates of the well fit objects are given in Table 5.

#### 5. Redshift evolution in properties

In Fig. 9 the parameters determined by several previous papers are presented. The first thing to note is the large spread in data points in this plot. The scatter in the results are partly due to different selection techniques (different Ly $\alpha$  flux and EW/colour constraints may bias the distribution of galaxy properties), and partly due to different SED fitting techniques. With the scatter taken into account, some trends are still visible. The dust parameter  $A_V$  would seem to undergo an interesting evolution; starting with large  $A_V$  at very high redshift, decreasing to almost no dust extinction at  $z \sim 3$ , and then increasing again. However, most of the very high redshift points do not have error bars, and the one that does exhibits a very large uncertainty in this parameter. We thus take this to mean that the dust extinction, or any of the stellar parameters, at very high redshift are not well constrained. Considering only the points at  $z \leq 3$  reveals increasing dust contents at lower redshifts. That the galaxies here are more dusty was predicted in Nilsson et al. (2009a, see also Guaita et al. 2010 for a similar result) based on the smaller equivalent widths and redder SEDs found in those papers. Further, LAEs at lower redshift are clearly more massive than at higher redshift. At both  $z = 0.3$  and  $2.3$ , stellar masses of the order or above  $10^{10} M_\odot$  are seen, whereas results at  $z > 3$  show stellar masses of  $\sim 10^9 M_\odot$  or lower. It should be noted that it has been shown that the masses of GALAXEV may be overestimated by a factor of two, using different stellar evolutionary codes (Maraston et al. 2006). Such an overestimate would still put these galaxies among the most massive Ly $\alpha$  emitters found to date. Both of these results, higher masses and more dust extinction, are also true when the fitting results from the total stack of LAE candidates is considered, i.e. the results are not biased towards the bright end of the luminosity function, but are true for the majority of the LAE candidates at  $z = 2.25$ .

We also note the cluster of points at ages of  $\sim 1.2$  Gyrs and stellar masses of  $\log M_\star \sim 10^{10} M_\odot$ . Four results can be



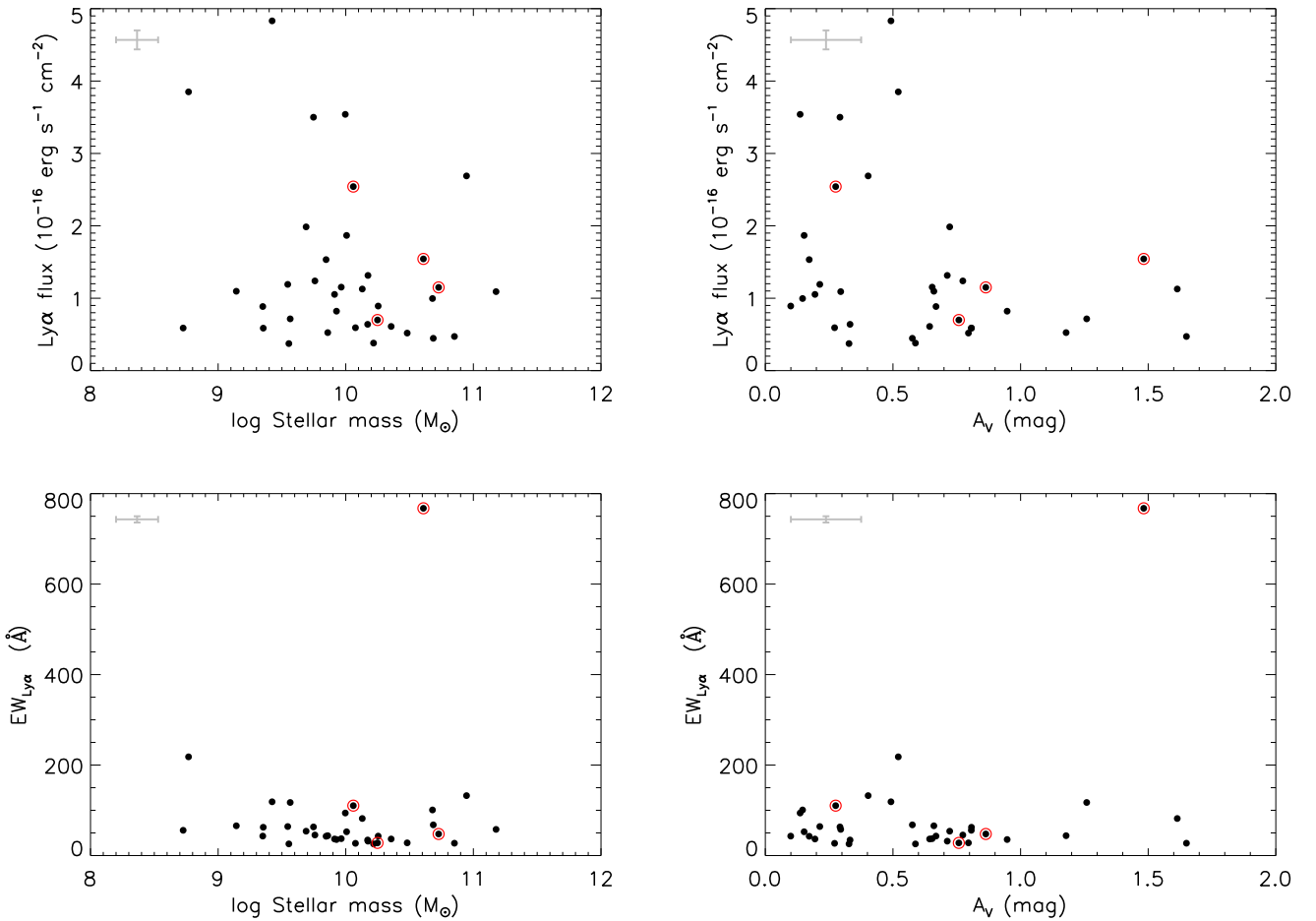


**Fig. 8.** Dependencies between Ly $\alpha$  flux (upper panels) and EW (lower panels) and best fitted stellar masses (left panels) and dust  $A_V$  (right panels). Typical error bars are marked in grey. ULIRGs are marked with a red ring. The very high EW object in the lower panels is LAE\_COSMOS\_94, see sec. 4.2.2. No clear dependencies are seen, besides a lack of objects at large Ly $\alpha$  fluxes and large extinctions.

found here, containing different percentages of the total samples; the light blue star comes from Lai et al. (2008) and is the fitting result of a stack of IRAC-detected LAEs at  $z = 3.1$ . Their IRAC-detected stack is the average of their 26% brightest/reddest sources. The dark blue circle is the mean of the SED fitting results at  $z = 0.3$  (Finkelstein et al. 2009b), containing 100% of their sample after confirmed AGN are removed. The black circle and star are the results from this publication, with the filled circle being the mean of the best fit parameters for the galaxies with a discernible older population, and the star the best fit parameters of the total stack. In this case, the total stack is made of all sources without AGN contamination, whereas the filled circle is the average of 69% of the galaxies with  $\chi_r^2 < 10$ . It thus appears that LAE surveys certainly find galaxies with different properties at different redshift, but that one particular type of galaxy (with an older population and  $\log M_{\star} \sim 10^{10} M_{\odot}$ ) is selected at all redshifts. At  $z = 0$  this appears to have become the canonical, and even type-defining, LAE which, however, was increasingly rarer at higher redshift.

Several difficult choices have to be made when preparing to fit the SEDs of a sample of high redshift galaxies, all of which may influence the final result (see also Gawiser et al. 2009). Firstly, the theoretical model must be chosen. We have here chosen the GALAXEV model, as this is most common in publications to date. Secondly, different groups fit different star formation histories (e.g. SSP, constant SFR, exponentially declining SFR) which may influence the results. As described in Sect. 3.1, nebular emission makes a strong contribution to the SED at very young ages, but this effect is typically not implemented in SED fitting codes. Some publications have included the narrow-band flux in the fitting, in an attempt to model the dust extinction more carefully (e.g. Finkelstein et al. 2008), whereas most groups tend to either ignore the data-point, or use it to subtract the Ly $\alpha$  flux from the broad-bands. Finally, one effect, which may be the more difficult to circumvent, is that of disparate restframe wavelength coverage at different redshifts. At higher redshifts, the fits rely increasingly on the *Spitzer* data points to constrain the restframe optical and near-infrared. The

uncertainty there lies in the low spatial resolution, and that, at fainter fluxes, the images quickly over-crowd.

## 6. Discussion

In this paper we have presented the results of fitting the SEDs of a set of Ly $\alpha$  emitters at  $z = 2.25$ . A first note to make is that the results presented here represent the single largest sample of individually studied Ly $\alpha$  emitters to date. This is for the simple reason that galaxies at  $z \sim 2$  are much more easily observable in the continuum than at higher redshifts. In Nilsson et al. (2009a), we proposed that LAEs at  $z \sim 2$  are dustier and more massive than at higher redshift, and that they contain more AGN. These suggestions are reinforced with the results presented here. With the new *Chandra* images, the number of detected AGN in the sample has increased to more than double what was found in Nilsson et al. (2009a). The LAEs in this sample have a typical  $A_V$  of  $\sim 0.5$  and a typical stellar mass of  $10^{10} M_\odot$ .

A strong anti-correlation was found between the age of the galaxy and the dust content in the Spearman rank test, with lower dust contents at older ages (see Table 6 and Fig. 6). It is remarkable that roughly half of the sample with a single young population have  $A_V > 1.0$ , whereas nearly all of the older objects have  $A_V < 1.0$ . Interestingly, few correlations were found between the Ly $\alpha$  properties of the galaxies, and their stellar masses or dust contents. The  $2\sigma$  anti-correlation between Ly $\alpha$  flux and  $A_V$ , with fainter Ly $\alpha$  fluxes at larger  $A_V$ , is a classic result, indicating that the extinction in general affects the Ly $\alpha$  emission in a strong negative way. Together with the correlation between age and  $A_V$ , it implies that the intrinsic Ly $\alpha$  emission in the young population must be much stronger than in the older population to survive the larger extinction. This is certainly possible, as these very young populations have a strong ionising continuum.

A possible explanation for the trend in dust contents with redshift is increasing metallicity. At very high redshift, we would expect the metallicity to be very low, consistent with low dust extinction and smaller stellar masses. An increasing metallicity at lower redshifts would then explain the increasing dust production and would be consistent with higher stellar masses, according to the mass-metallicity correlation (e.g. Tremonti et al. 2004). Unfortunately, the measurements of our SEDs, alternatively the accuracies of the stellar models, are not enough to constrain the metallicity in the SED fits. For this measurement, accurate line ratios between restframe optical emission lines are needed and could in the future be measured with e.g. the X-shooter instrument at ESO/VLT.

It may be argued that the results presented here are biased to the brightest end of the galaxy sample, in that only objects individually detected in the redder bands are fitted. For example, summing the average stellar mass found for the total stack, and comparing it to the sum of the individually fit objects (sec. 4.2), we find that those 20% of the candidates contain 50% of the total stellar mass among the galaxies. These 20% are obviously among the brightest, although the secondary criteria of having small  $\chi_r^2$  is also imposed. However, the same bias exists in all other similar campaigns to understand the properties of high

redshift galaxies. For this reason we also chose to fit the stacked fluxes, which should reveal results in a consistent manner to results reported for LAEs at high redshift. For the total stack of KPNO  $K_s$  non-detected objects, the dust was found to be  $A_V = 0.28_{-0.16}^{+0.46}$  compared to  $0.26_{-0.17}^{+0.11}$  for the  $z \sim 3$  LAEs in Nilsson et al. (2007) and  $0.0_{-0.0}^{+0.1}$  in Gawiser et al. (2007). The red stack was better fitted with more dust ( $A_V = 0.43_{-0.21}^{+0.57}$ ) and the blue stack with less dust ( $A_V = 0.12_{-0.09}^{+0.25}$ ). Thus the results indicate that lower redshift LAEs are likely to have a larger dust content, but many galaxies are still relatively dust-free. As for the stellar masses, the stacked average masses found at  $z \sim 3$  are of the order  $0.5 - 1.0 \times 10^9 M_\odot$ , whereas the total stack here was best fitted with an average mass of  $\sim 7 \times 10^9 M_\odot$ , almost a factor of ten larger. If this is a selection effect based on the shallow flux limit, then an extremely large population of low mass, low flux LAEs would have to exist at redshift two, to get an average mass similar to the observations at redshift three.

Further, we see no evidence for two populations of LAEs, with a red and a blue sub-sample. Instead, the results in Fig. 6 follow a smooth transition from little to a large amount of dust, and from smaller to larger masses. If a flux cut was made in our sample at a higher flux, only the most massive objects would be individually detected. The stack of the remaining objects would be dominated by smaller mass objects and so if this stack is also fitted for, it would appear as though there was a dichotomy of LAE classes. The smooth transition of properties seen in the sample here rather indicates that Ly $\alpha$  emitters can be found in any type of galaxy at  $z = 2.25$ .

The apparent shift in stellar properties with redshift is easily explained with a simple, phenomenological model when considering which objects in the Universe emit Ly $\alpha$  photons. At high redshift ( $z > 3$ ), most galaxies are small and in their first star formation episode. AGN and ULIRG number densities are low. Most Ly $\alpha$  photons at this stage in time will thus trace this; young, small star-forming galaxies in their first starburst, with little dust content. Very few AGN or ULIRG LAEs will be found. A Gyr later, at  $z \sim 2$ , both the star formation rate density and the AGN number density are peaking. Some galaxies are already in their second, or later, starburst. Now the sample of Ly $\alpha$  selected galaxies will reflect this diversity, with more AGN and ULIRG LAEs detected and a larger range of stellar properties. Whereas there will be some galaxies in the same stage of evolution as at higher redshift, there will also be some galaxies with evolved stellar populations that are experiencing more recent star formation. These galaxies can be more massive and/or more dusty. Thus, Ly $\alpha$  emitters are not a homogeneous type of high redshift galaxy, certainly less so than i.e. Lyman-Break galaxies (Nilsson et al., *subm. to A&A*). Selecting by Ly $\alpha$  emission will, and does, find a cross-section of Ly $\alpha$  emitting objects at each redshift and even though this technique is complementary to other high redshift galaxy selection techniques, the most valuable comparisons are probably with other galaxies at the same redshift. For example, Shapley et al. (2005) found that LBGs at  $z \sim 2$  had stellar masses  $\log M_* = 10.8 M_\odot$ ,  $A_V = 0.86$  mag and ages around 1 Gyr, with 15% having very young ages ( $< 100$  Myrs). These val-

ues are more consistent with the results found for LAEs here, than comparing LAE results at different redshifts. The study of the redshift evolution of LAEs can thus be seen as an evolution in Ly $\alpha$  emission in the Universe, and could as such be an interesting test for galaxy evolution models including both star formation, dust effects and AGN number densities.

## 7. Conclusion

Based on the work presented here, studying the photometric properties of  $z = 2.25$  LAEs, and fitting the SEDs of the objects with spectral templates, the following conclusions can be made.

- LAEs at  $z = 2.25$  are generally more massive and more dusty than at higher redshift, and their properties are quite diverse

Using a sophisticated MCMC fitting method, the stellar properties were derived for 36 well-fit objects, as well as three stacks. The LAEs were typically best fit with  $A_V = 0.0 - 2.0$  mag and  $\log M_* = 9.0 - 11.0 M_\odot$ . We have shown that when multiple populations of stars exist in the galaxies, the older populations are often outshone by the younger. Roughly 40% of the LAEs studied here are in such a strong star-bursting phase that any other older populations are invisible, whereas the remaining 60% have “confirmed” older populations of stars. In section 5 we showed that LAEs at higher redshift ( $z > 3$ ) tend to have smaller masses and dust contents.

- Larger AGN fraction among LAEs

An analysis of the *Chandra* X-ray images available in COSMOS revealed 11 new AGN detections, increasing the AGN fraction in this LAE sample to 13%.

- Stacking of objects does not reveal the average of the properties of the individual objects

SED fitting of high redshift galaxies is typically done on stacks of objects. We tested here the assumption that the stack reveals the average of the individual results. By stacking the individually best fit 36 objects, we showed that the fitted stellar properties of this stack were not the average of the properties of the individual objects. In the process of stacking, the light from multiple populations of stars is smeared out, and particularly the age determination becomes highly uncertain.

- Anti-correlations between ages and  $A_V$ , and Ly $\alpha$  flux and  $A_V$ , were seen

An anti-correlation between the age and  $A_V$  with 99.97% probability was detected among the 36 individually fitted objects. A further anti-correlation between Ly $\alpha$  flux and  $A_V$ , with 94.8% probability, was also seen, confirming the long-standing prediction that, on average, more dust results in less Ly $\alpha$  escape in high redshift galaxies.

*Acknowledgements.* The Dark Cosmology Centre is funded by the DNRF. GÖ is a Royal Swedish Academy of Sciences research fellow, supported through a grant from the Knut and Alice Wallenberg foundation, and also acknowledges support from the Swedish research council and the Swedish national space board.

## References

- Baade, D., Meisenheimer, K., Iwert, O., et al., 1999, *The Messenger* 95, 15
- Blain, A.W., Smail, I., Ivison, R.J., Kneib, J.-P., 1999, *MNRAS*, 302, 632
- Bloom, J.S., Djorgovski, S.G., Kulkarni, S.R., & Frail, D.A., 1998, *ApJ*, 507, L25
- Bongiovanni, Á, Oteo, I., Cepa, J., et al., 2010, accepted in *A&A*, arXiv:1008.1753
- Bruzual G.A., Charlot S., 2003, *MNRAS*, 344, 1000
- Calzetti, D., Armus, L., Bohlin, R.C., et al., 2000, *ApJ*, 533, 682
- Chapman, S.C., Blain, A.W., Smail, I., & Ivison, R.J., 2005, *ApJ*, 622, 772
- Christensen, L., Hjorth, J., & Gorosabel, J., 2004, *A&A*, 425, 913
- Colbert, J.W., Teplitz, H., Francis, P., et al., 2006, *ApJ*, 637, L89
- Cowie, L.L., & Hu, E.M., 1998, *AJ*, 115, 1319
- Daddi, E., Cimatti, A., Renzini, A., et al., 2004, *ApJ*, 617, 746
- Elvis, M., Civano, F., Vignali, C., et al., 2009, *ApJS*, 184, 158
- Finkelstein, S.L., Rhoads, J.E., Malhotra, S., Pirzkal, N., & Wang, J., 2007, *ApJ*, 660, 1023
- Finkelstein, S.L., Rhoads, J.E., Malhotra, S., Grogin, N., & Wang, J., 2008, *ApJ*, 678, 655
- Finkelstein, S.L., Rhoads, J.E., Malhotra, S., & Grogin, N., 2009a, *ApJ*, 691, 465
- Finkelstein, S.L., Cohen, S.H., Malhotra, S., & Rhoads, J.E., 2009b, *ApJ*, 700, 276
- Finkelstein, S.L., Cohen, S.H., Malhotra, S., Rhoads, J.E., & Papovich, C., 2009c, *ApJ*, 703, L162
- Finkelstein, S.L., Cohen, S.H., Windhorst, R.A., et al., 2010, submitted to *ApJ*, arXiv:1008.0634
- Franx, M., Labbé, I., Rudnick, G., et al., 2003, *ApJ*, 587, L79
- Fynbo, J.P.U., Møller, P., & Thomsen, B. 2001, *A&A* 374, 443
- Fynbo, J.P.U., Møller, P., Thomsen, B., et al., 2002, *A&A*, 388, 425
- Förster Schreiber, N.M., van Dokkum, P.G., Franx, M., et al., 2004, *ApJ*, 616, 40
- Gawiser, E., Van Dokkum, P.G., Gronwall, C., et al., 2006, *ApJL*, 642, 13
- Gawiser, E., Francke, H., Lai, K., et al., 2007, *ApJ*, 671, 278
- Gawiser, E., 2009, *NAR*, 53, 50
- Giavalisco, M., 2002, *ARAA*, 40, 579
- Gronwall, C., Ciardullo, R., Hickey, T., et al., 2007, *ApJ*, 667, 79
- Grove, L.F., Fynbo, J.P.U., Ledoux, C., et al., 2009, *A&A*, 497, 689
- Guaita, L., Gawiser, E., Padilla, N., et al., 2010, *ApJ*, 714, 255
- Hayes, M., Östlin, G., Atek, H., et al., 2007, *MNRAS*, 382, 1465
- Hornschemeier, A.E., Brandt, W.N., Garmire, G.P., et al., 2001, *ApJ*, 554, 742
- Ilbert, O., Capak, P., Salvato, M., et al., 2009, *ApJ*, 690, 1236
- Ivison, R.J., Smail, I., Le Borgne, J.-F., et al., 1998, *MNRAS*, 298, 583
- Ivison, R.J., Smail, I., Barger, A.J., et al., 2000, *MNRAS*, 315, 209
- Kennicutt, R.C., 1998, *ARAA*, 36, 189
- Lai, K., Huang, J.-S., Fazio, G., et al., 2007, *ApJ*, 655, 704
- Lai, K., Huang, J.-S., Fazio, G., et al., 2008, *ApJ*, 674, 70
- Leitherer, C., Schaerer, D., Goldader, J.D., et al., 1999, *ApJS*, 123, 3
- Madau, P., Ferguson, H.C., Dickinson, M.E., et al., 1996, *MNRAS*, 283, 1388
- Maraston, C., Daddi, E., Renzini, A., et al., 2006, *ApJ*, 652, 85
- Møller, P., & Warren, S.J., 1998, *MNRAS*, 299, 661
- Muzzin, A., Marchesini, D., van Dokkum, P.G., et al., 2009, *ApJ*, 701, 1839
- Nilsson, K.K., Møller, P., Möller, O., et al., 2007, *A&A*, 471, 71
- Nilsson, K.K., Tapken, C., Møller, P., et al., 2009a, *A&A*, 498, 13

- Nilsson, K.K., Möller-Nilsson, O., Møller, P., Fynbo, J.P.U., & Shapley, A.E., 2009b, MNRAS, 400, 232
- Nilsson, K.K., & Møller, P., 2009, A&A, 508, L21
- Ouchi, M., Shimasaku, K., Okamura, S. et al., 2004, ApJ, 611, 685
- Ouchi, M., Shimasaku, K., Akiyama, M., et al., 2008, ApJS, 176, 301
- Papovich, C., Dickinson, M., & Ferguson, H.C., 2001, ApJ, 559, 620
- Papovich, C., Moustakas, L.A., Dickinson, M., et al., 2006, ApJ, 640, 92
- Pentericci, L., Grazian, A., Fontana, A., et al., 2009, A&A, 494, 553
- Pirzkal, N., Malhotra, S., Rhoads, J.E., & Xu, C., 2007, ApJ, 667, 49
- Raiter, A., Fosbury, R.A.E., & Teimoorinia, H., 2010, A&A, 510, 109
- Reddy, N.A., Erb, D.K., Steidel, C.C., et al., 2005, ApJ, 633, 748
- Reddy, N.A., Steidel, C.C., Erb, D.K., Shapley, A.E., & Pettini, M., 2006, ApJ, 653, 1004
- Sanders, D.B., Salvato, M., Aussel, H., et al., 2007, ApJS, 172, 86
- Schaerer, D., 2003, A&A, 397, 527
- Schmidt, M., Hasinger, G., Gunn, J., et al., 1998, A&A, 329, 495
- Shapley, A.E., Steidel, C.C., Erb, D.K., et al., 2005, ApJ, 626, 698
- Steidel, C.C., Giavalisco, M., Pettini, M., Dickinson, M., & Adelberger, K.L., 1996, ApJ, 462, L17
- Steidel, C.C., Adelberger, K.L., Giavalisco, M., Dickinson, M., & Pettini, M., 1999, ApJ, 519, 1
- Tremonti, C.A., Heckman, T.M., Kauffman, G., et al., 2004, ApJ, 613, 898
- Tumlinson, J., Shull, J.M., & Venkatesan, A., 2003, ApJ, 584, 608
- Venemans, B.P., Röttgering, H.J.A., Miley, G.K., et al., 2007, A&A, 461, 823
- Verma, A., Lehnert, M.D., Förster-Schreiber, N.M., Bremer, M.N., & Douglas, L., 2007, MNRAS, 377, 1024
- Wang, J.X., Rhoads, J.E., Malhotra, S., et al., 2004, ApJL, 608, 21
- Yuma, S., Ohta, K., Yabe, K., et al., 2010, accepted in ApJ, arXiv:1007:2057
- Zackrisson, E., Bergvall, N., & Leitert, E., 2008, ApJ, 676, L9
- Östlin, G., Hayes, M., Kunth, D., et al., 2009, AJ, 138, 923

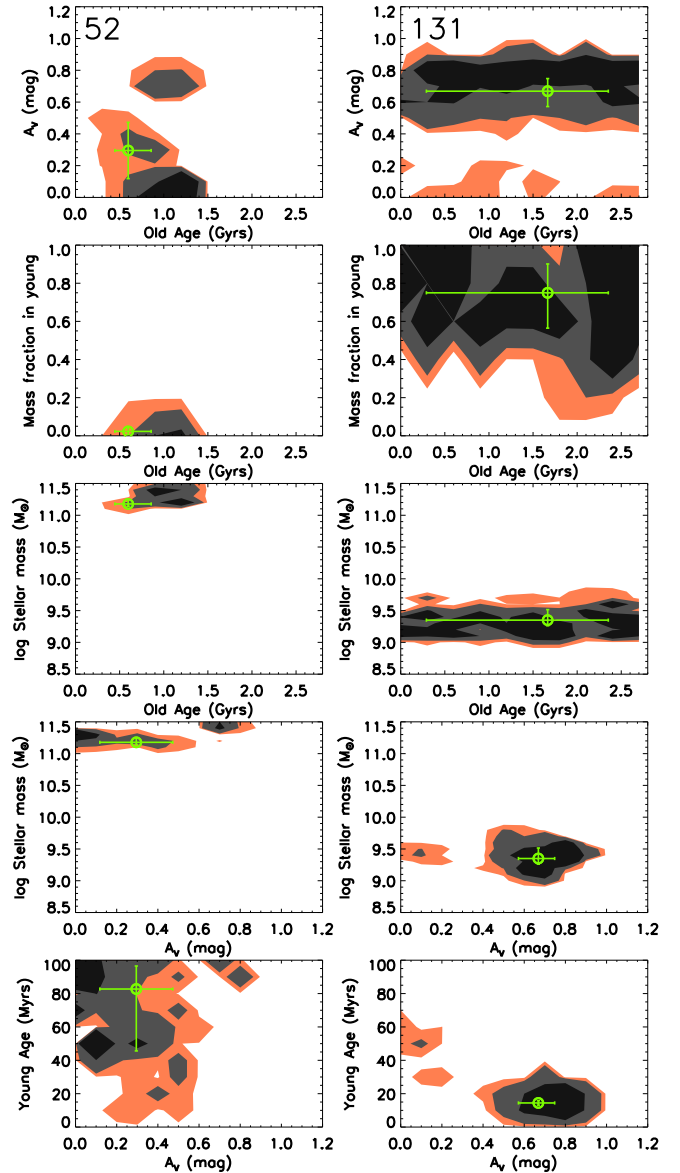


**Fig. 3.** Parameter dependencies between old/young population age, mass fraction, dust  $A_V$  and stellar mass for LAE\_COSMOS\_52 (*left*) and LAE\_COSMOS\_131 (*right*). Contours mark 68%, 95% and 99.7% probability. The green point marks the median of the parameter, with the  $1\sigma$  error bar as found in Table 5. For the object in the left panels, the stellar mass is well constrained. The mass fraction in the young population is low, and hence the older population age is also well constrained. In this case, the younger population has a larger span of possible solutions, partially dependent on the  $A_V$ , which appears to have two possible solutions. This is an example of a galaxy for which the older population age is observed, as opposed to the object on the right. Here, the stellar mass and  $A_V$  are well constrained, but the young population age is very young, and the mass fraction in the young population is allowed to be any value above  $\sim 25\%$ . Hence, the older population age is completely unconstrained.



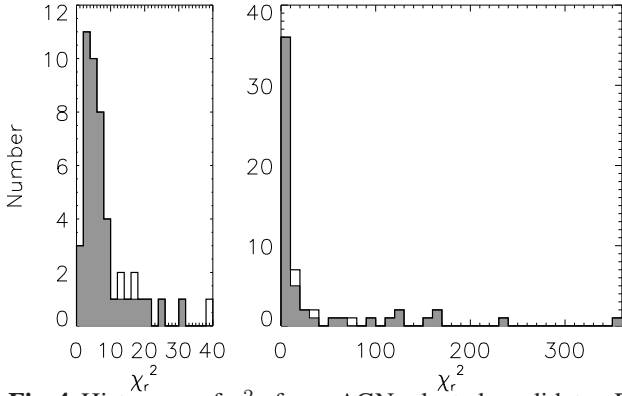


**Fig. 4.** Histogram of  $\chi_r^2$  of non-AGN selected candidates. Right panel shows complete distribution with a bin size of 10, left panel a zoom on the range  $0 - 40 \chi_r^2$  with a bin size of 2. Filled histogram are for candidates that are not detected in the GALEX data.

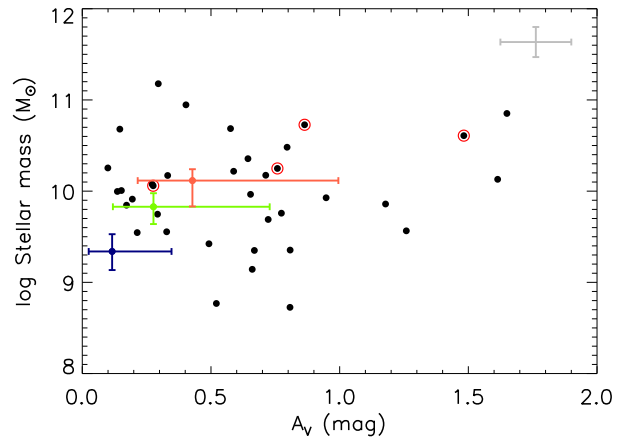
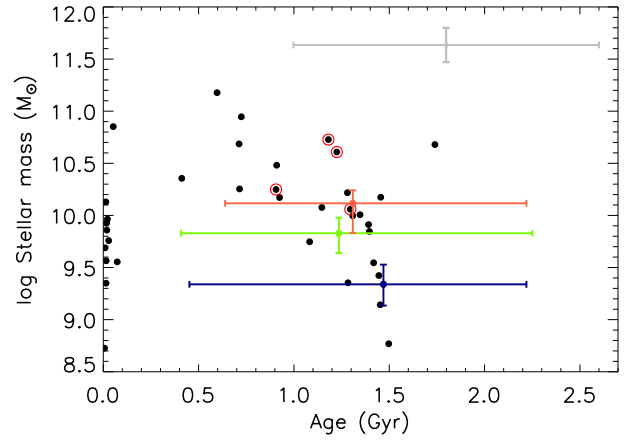
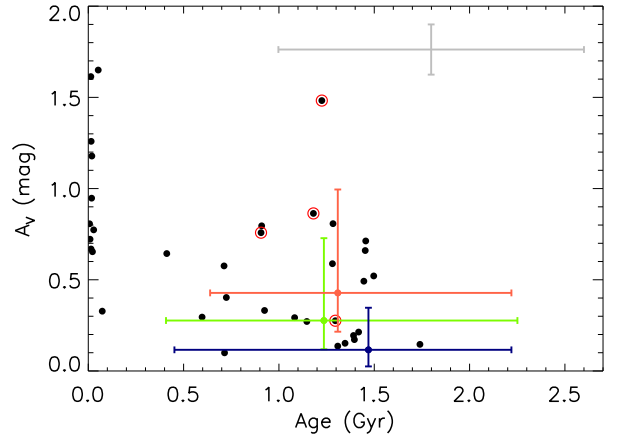


**Fig. 6.** Results of 36 non-AGN or GALEX detected sources with  $\chi_r^2 < 10$  (black points). The coloured data points represent the stacked SEDs, with green as the total non- $K_s$  detected sample, red and blue points are the red and blue sub-samples. Typical error bars are marked in grey. In the two top panels the error bars in the “Age” direction refer to those with ages above 100 Myrs. For the single young population objects, the typical error in age is  $\sim 15$  Myrs. LAE ULIRGs (from Nilsson & Møller 2009) are marked with a red ring.

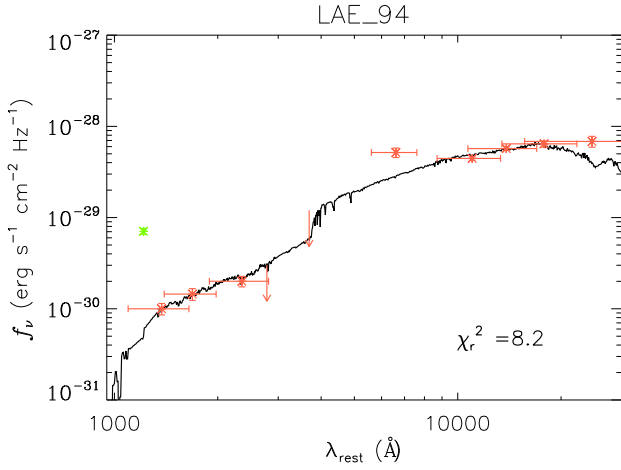


**Fig. 7.** SED of LAE\_COSMOS\_94. It is very faint in the broadbands, although with a large Ly $\alpha$  flux, and a very red SED in the *Spitzer* bands. Red points are observed data-points, arrows mark upper limits. The solid line shows the best fit spectrum. The green data point is the narrow-band flux (Ly $\alpha$ ) for reference.

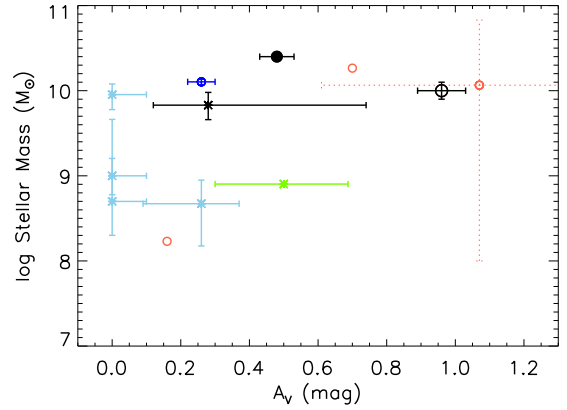
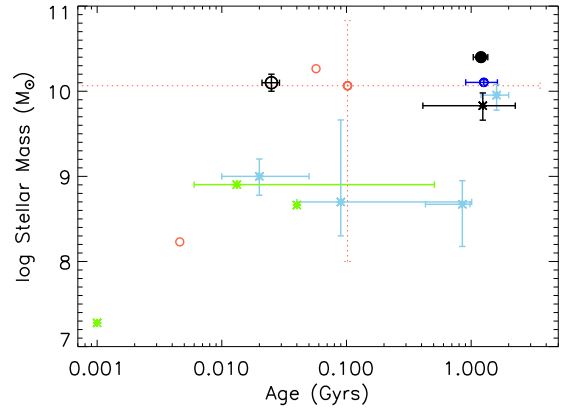
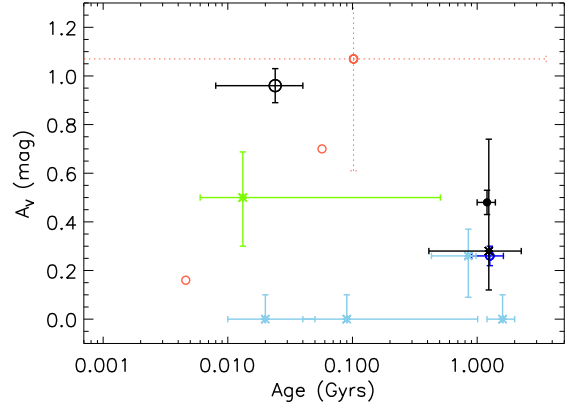


**Fig. 9.** SED properties derived in several publications at different redshifts; at  $z \sim 3$  with light blue points from Gawiser et al. (2006, 2007), Nilsson et al. (2007) and Lai et al. (2008). Green points are at  $z \sim 4.5$  from Finkelstein et al. (2007, 2009a). Red points are at  $z \sim 5.7$  from Lai et al. (2007) and Pirzkal et al. (2007), and at  $z \sim 4.9$  from Yuma et al. (2010). The dark blue point is the mean of a sample of  $z \sim 0.3$  LAEs from Finkelstein et al. (2009b), with confirmed AGN excluded (Finkelstein et al. 2009c). Circle points refer to mean results for individually fitted objects, whereas the star points refer to results from fitting stacks of objects. The black circles marks the mean in our sample of 36 best fit candidates; the filled circle is for the subsample with two populations and the open circle is for the single (young) population galaxies. The black star is the result of the fit of the total stack of LAEs at  $z = 2.25$ . Points without error bars were published without these values.